Application of Potential Theory in Calculating Wave-Induced Vertical Forces on Horizontal Cylinders Near a Plane Boundary

Tomasz Marcinkowski[*], Piotr Wilde[**]

[*]Gdańsk University of Technology, Faculty of Civil and Environmental Engineering,
ul. G. Narutowicza 11/12, 80-952 Gdańsk, Poland, e-mail: tmar@pg.gda.pl
[**]Polish Academy of Sciences, Institute of Hydro-Engineering (IBW PAN)
ul. Kościerska 7, 80-328 Gdańsk, Poland

Abstract

Hydrodynamic forces acting on a horizontal cylinder located in the vicinity of the bottom are analyzed by a diffraction theory which solves the problem in terms of a velocity potential. The cylinder is assumed to be rigidly anchored to the bottom at a sufficient depth, so that it has no influence on the surface profile. The potential function ϕ is defined as the sum of the incident wave velocity potential ϕ^w and the scattered wave velocity potential ϕ^a. The results of measurements of wave-induced pressures and forces on a horizontal cylinder located close to the bottom are compared with the theoretical solution based on the potential theory for incompressible, perfect fluid and ideal boundary conditions at the bottom and the surface of the cylinder. The experiments were carried out in the Large Wave Channel in Hannover with a cylinder of 0.8 m diameter. Thus the results are in a scale which corresponds to real pipelines. The analysis shows that the potential theory explains the components with double frequency of the wave in pressures and vertical forces as far as the amplitudes are concerned. In the experiments, the Keulegan-Carpenter number is rather low and the inertia hydrodynamic forces on the cylinder are dominant. It seems that the observed phase shift between the force component and the wave results from the energy dissipation which is not considered in the theoretical solution.

Key words: hydrodynamic forces, underwater pipeline, potential theory, diffraction theory, curvilinear coordinates

1. Introduction

The problem of flow around a cylinder has a long history. A good summary of solutions of the potential theory in complex function formulation is given by Müller (1928). This theory is used in the analysis of cylinders near a plane bottom by Carpenter (1958), Yamamoto et al (1974), Wright and Yamamoto (1979), Chakrabarti (1987), Sumer and Fredsøe (1997).

One cannot expect a perfect solution within the potential theory for incompressible, perfect fluid and ideal boundary conditions. Further assumption is that the ratio of the submerged depth to the cylinder radius is big enough, so the influence of the reflection on the free surface elevation can be neglected. Therefore, this solution cannot describe the complicated real behaviour. The authors believe that viscosity must be important, especially for processes near the seabed in connection with a cylinder; even more, the vortex shedding at the cylinder and bottom might have a considerable influence. Nevertheless the present theory seems to be useful in explaining some other features. However, the application of the theory in complex function formulation is difficult as far as extension is concerned. Therefore, the authors decided to look at the solution by applying curvilinear coordinates. A good and useful presentation of curvilinear coordinates is given by Moon and Spencer (1971).

2. Theoretical Consideration

The bi-cylindrical coordinates form the traditional coordinate system, suitable for the discussed problem (Fig. 1). The cartesian coordinates x, y are expressed in terms of the bi-cylindrical coordinates u and v by the following relations:

$$x = \frac{a \cdot \sinh u}{\cosh u - \cos v}, \quad y = \frac{a \cdot \sin v}{\cosh u - \cos v}, \tag{1}$$

where a is a constant.

The parameters depend on the radius of the cylinder being R and the gap between the cylinder and the bottom e (Fig. 1). From these conditions follows:

$$\cosh u_R = 1 + \frac{e}{R}, \quad a = R \sinh u_R, \tag{2}$$

where u_R is the value of the coordinate u for which $x(v)$ and $y(v)$ describe the surface of the cylinder with v in the interval $(-\pi, \pi)$. When gap e goes to zero, expressions (1) yield unidentified values. Let us introduce new variables u^* and v^* by the following definition:
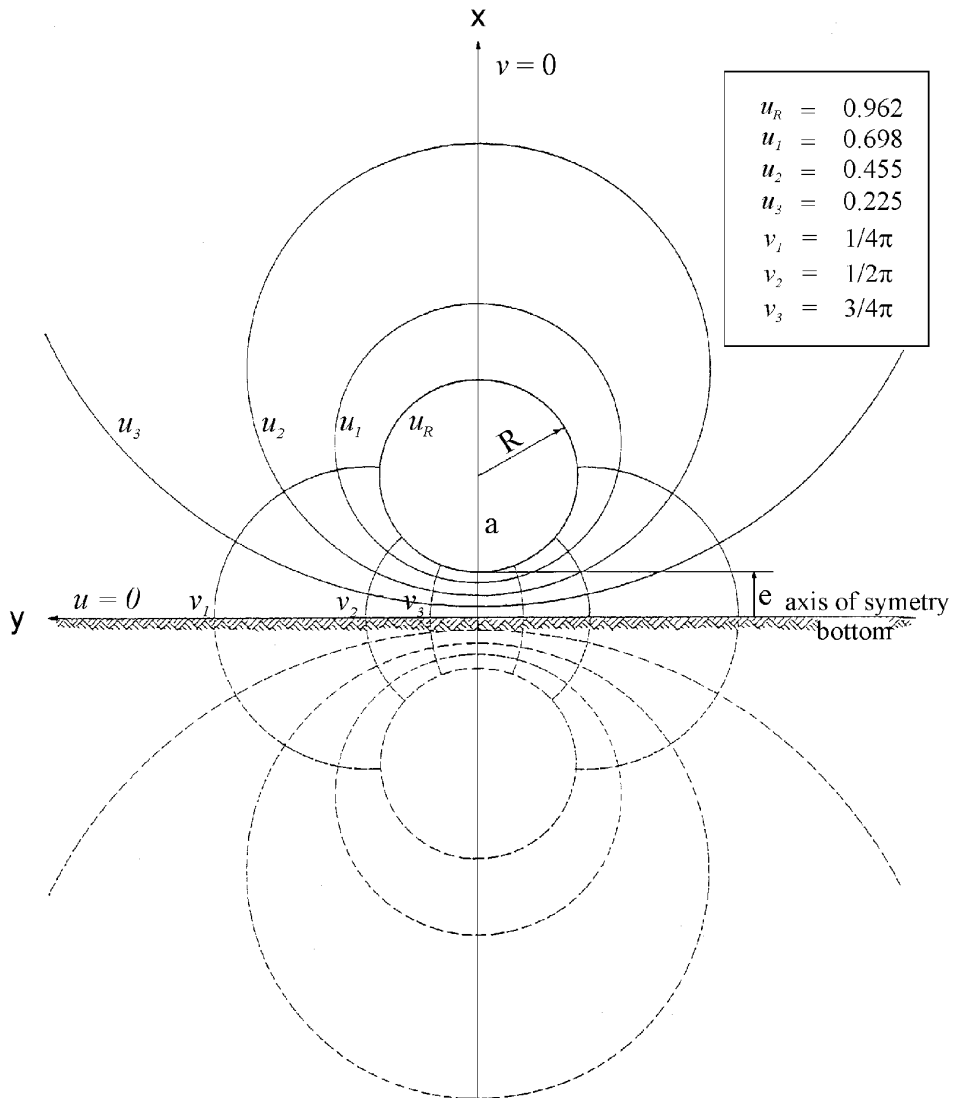
$$u = \sqrt{\frac{2e}{R}} \, u^*, \quad v = \sqrt{\frac{2e}{R}} \, v^*. \tag{3}$$

When e goes to zero the new variables have limits; appropriate calculations lead to the following expressions for the curvilinear coordinates (1):

$$x = \frac{2Ru^*}{u^{*2} + v^{*2}}, \quad y = \frac{2Rv^*}{u^{*2} + v^{*2}}. \tag{4}$$

The relations obtained are the corresponding expressions for the tangential cylinder coordinates multiplied by $2R$ (Moon and Spencer 1971). The surface of

x

$v = 0$

u_R	$=$	0.962
u_1	$=$	0.698
u_2	$=$	0.455
u_3	$=$	0.225
v_1	$=$	$1/4\pi$
v_2	$=$	$1/2\pi$
v_3	$=$	$3/4\pi$

u_3 u_2 u_1 u_R

R

a

$u = 0$ v_1 v_2 v_3

y

e axis of symetry

bottom

Example:

R = 0.4 [m]   -   radius of the cylinder

e = 0.2 [m]   -   gap between cylinder and plane boundary

Fig. 1. Bipolar coordinate system

the cylinder corresponds to $u_R^* = 1$. It is obvious from the above, that an analysis for small gaps has to be carried out carefully as the transition goes through unidentified symbols.
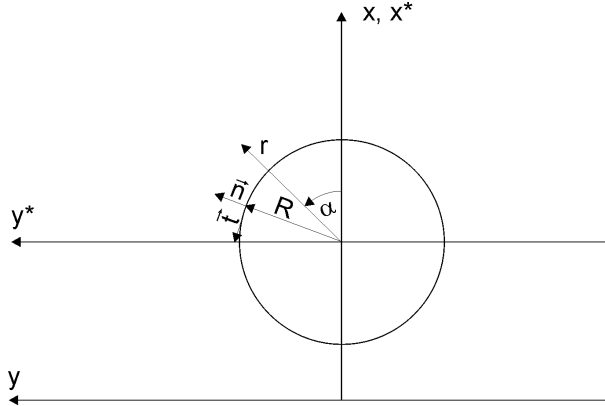

Fig. 2. Sign convention

In the analysis it is convenient to work simultaneously with polar coordinates as shown in Fig. 2. It follows that:

$$\sin \alpha = \frac{\sqrt{\frac{2e}{R}(1 + \frac{e}{R})}}{1 + \frac{e}{R} - \cos v} \sin v, \quad \cos \alpha = \frac{(1 + \frac{e}{R}) \cos v - 1}{1 + \frac{e}{R} - \cos v} \tag{5}$$

and for the limiting case $e \to 0$:

$$\sin \alpha = \frac{2v^*}{1 + v^{*2}}, \quad \cos \alpha = \frac{1 - v^{*2}}{1 + v^{*2}}. \tag{6}$$

The points $v = 0$ and $v^* = 0$ are at the top of cylinder and correspond to $\alpha = 0$. Points $v = \pi$ and $v^* \to \infty$ are at the bottom of the cylinder and correspond to $\alpha = \pi$.

The bi-cylindrical and tangential cylinder coordinate systems are orthogonal, and the corresponding metric tensors are:

$$\sqrt{g_{uu}} = \sqrt{g_{vv}} = \frac{a}{\cosh u - \cos v}, \tag{7}$$

$$\sqrt{g_{u^*u^*}} = \sqrt{g_{v^*v^*}} = \frac{2R}{u^{*2} + v^{*2}}. \tag{8}$$

If ϕ is a potential function and $\overrightarrow{n}$ denotes a unit outward normal to the cylinder and $\overrightarrow{t}$ is a unit tangential vector which points in the direction of the increase of α, then the normal and tangential velocity components are expressed by the formulae:

$$v_n = -\frac{1}{\sqrt{g_{uu}}}\frac{\partial\phi}{\partial u}, \quad v_t = \frac{1}{\sqrt{g_{uu}}}\frac{\partial\phi}{\partial v}. \tag{9}$$

The potential function for the perfect fluid satisfies the Laplace equation, which in bi-cylindrical coordinates takes the following form:

$$\frac{1}{g_{uu}}\left[\frac{\partial^2\phi}{\partial u^2} + \frac{\partial^2\phi}{\partial v^2}\right] = 0. \tag{10}$$

The same relations as given in (9) and (10) are true for the tangential cylindrical coordinates when u and v are replaced by u^* and v^*.

As $g_{uu} \neq 0$ and $g_{u^*u^*} \neq 0$, it follows from equation (10) that the Laplace equation has the same form in both curvilinear coordinate systems and a cartesian coordinate system. The same solution obtained by the separation of variables may be applied to the curvilinear coordinate systems. For the case considered in this paper, the appropriate solution in terms of a Fourier series which satifies the Laplace equation is:

$$\phi = A \cdot u + \sum_{r=1}^{\infty} \cosh(ru)[A_r \cos(rv) + B_r \sin(rv)]. \tag{11}$$

The normal velocity component at the cylinder surface v_n^a given by equation (9) with the potential ϕ yields:

$$v_n^a = -\frac{1}{\sqrt{g_{uu}}}\left\{A + \sum_{r=1}^{\infty} r \cdot \sinh(ru_R)[A_r \cos(rv) + B_r \sin(rv)]\right\}. \tag{12}$$

The sums of the normal velocity components – one resulting from approaching waves (denoted by v_n^w) and the other resulting from additional potential (denoted by v_n^a) – are equal to zero at each point on the cylinder surface.

The values of constants A, A_r, B_r are calculated by numerical method while the values of normal velocity components v_n^a are defined by taking a limited number of series elements according to equation (12). Hence it is advisable to introduce a clearly defined measure of solution accuracy. The measure in question may be written in the following integral form:

$$J = \int_{-\pi}^{\pi} W(v)\left[v_n^w(v) + v_n^a(v)\right]^2 ds = 0, \tag{13}$$

where $ds = \sqrt{g_{vv}}dv$ is the elementary arc length and $W(v)$ a weighting function which must be positive in the range of $(-\pi, \pi)$. For an exact solution, the function under the integral is zero, and thus J is a minimum value. The necessary condition for J to become a minimum value means that all derivatives with respect to A,

A_r and B_r must be equal to zero. From using the function $\sqrt{g_{vv}}$ as a weighting function $W(v)$ it follows that:

$$A = \frac{1}{\pi} \int\limits_{-\pi}^{\pi} v_n^w \sqrt{g_{vv}} dv,$$

$$A_n = \frac{1}{n \sinh(nu_R)} \frac{1}{\pi} \int\limits_{-\pi}^{\pi} v_n^w \cos(nv) \sqrt{g_{vv}} dv, \qquad (14)$$

$$B_n = \frac{1}{n \sinh(nu_R)} \frac{1}{\pi} \int\limits_{-\pi}^{\pi} v_n^w \sin(nv) \sqrt{g_{vv}} dv.$$

The above-mentioned integrals have generally to be calculated by a numerical method. For standard calculations, the interval 2π for v has been divided into 360 parts and two different numerical procedures were applied for the calculation of the Fourier coefficients.

For an approximated calculation, a measure of accuracy must be introduced. When calculating the coefficients A, A_r, B_r, the values of v_n^a were evaluated by means of the equation (12) and the value of J was determined by a numerical method. This value should be zero for an exact solution. The square root of J is therefore considered a good measure. In order to obtain a relative measure, this value J, which was also used for other calculations, was divided by the square root of the integral (13) when $v_n^a(v)$ was disregarded. The value of this measure was in the order of 10^{-4} for the numerical calculations, but increased for very small gaps. For that reason the interval had to be divided into more parts than before, and the number of Fourier coefficients considered had also to be increased.

The Fourier series may be written in complex number notation by introducing a complex number Fourier coefficient $A_n + i B_n$ where $i = \sqrt{-1}$.

The final formula with the variables u^* and v^* defined by equation (3) has the following form:

$$\phi = \frac{R\sqrt{1 + \frac{e}{2R}}}{\pi} \sum_{-\infty}^{\infty} \frac{\cosh(\zeta_n u^*)}{\zeta_n \sinh(\zeta_n u_R)} \sqrt{\frac{2e}{R}} \int\limits_{-\pi\sqrt{\frac{R}{2e}}}^{\pi\sqrt{\frac{R}{2e}}} \frac{v_n^w \exp(i\zeta_n w^*)}{1 + \frac{R}{e}\left[1 - \cos\left(\sqrt{\frac{2e}{R}} w^*\right)\right]} \times \qquad (15)$$
$$\times \, dw^* \exp(-i\zeta_n v^*),$$

where w^* is a dummy variable of integration and $\zeta_n = n\sqrt{\frac{2e}{R}}$.

When $e/R \to 0$, then $\zeta_n \to \zeta$ in continuum, $\sqrt{\frac{2e}{R}} \to d\zeta$ and the sum goes over to the integral from $-\infty$ to ∞. Finally it follows that:

$$\phi = \frac{R}{\pi} \int\limits_{-\infty}^{\infty} \frac{\cosh(\zeta u^*)}{\zeta \sinh \zeta} \int\limits_{-\infty}^{\infty} \frac{v_n^w \exp(i\zeta w^*)}{1 + w^{*^2}} \, dw^* d\zeta. \tag{16}$$

The solution of the Fourier series then goes over to the Fourier integral solution.

The same solution may be obtained by the standard procedure which leads to the Fourier integral transform of the Laplace equation and the boundary condition. It follows from these calculations that the Fourier transform of $\phi(u^*, v^*)$ is:

$$F(u^*, \zeta) = \frac{2R}{\sqrt{2\pi}} \frac{\cosh(\zeta u^*)}{\zeta \sinh(\zeta u_R^*)} \int\limits_{-\infty}^{\infty} \frac{v_n^w \exp(i\zeta w^*)}{1 + w^{*^2}} dw^*, \tag{17}$$

and the inverse transformation is:

$$\phi(u^*, v^*) = \frac{1}{\sqrt{2\pi}} \int\limits_{-\infty}^{\infty} F(u^*, \zeta) \exp(-i\zeta v^*) d\zeta. \tag{18}$$

The above result corresponds exactly with the relation (16).

The difficulties which arise when a finite gap comes over to the case of a cylinder welded at the bottom, appear in the numerical calculations for very small gaps compared to the radius of the cylinder.

3. Comparison of Theoretical Results with Experimental Data

The problem of wave forces on a cylinder is, among others, discussed by Sarpkaya and Isaacson (1981). The formulae used in engineering practice are of a semi-empirical nature and the understanding of the mechanics is far from being complete.

Comparing theoretical and experimental results we follow Bowie (1977) in the sense that we compare the time-dependent Fourier components obtained from the theoretical treatment with those obtained from data processing of the measured time sequences.

In the theoretical treatment, it was assumed that the waves can be described by Stokes' second order theory. Thus the potentials of approaching waves are the sum of two terms with frequencies ω and 2ω in time. The normal velocity components were calculated at the surface of the cylinder from the solution of the wave problem in the layer without the cylinder for the first and second term.

For these terms, the Fourier coefficients were determined by numerical integration and the value of the potentials and tangential velocities of the imaginary cylinder were determined. The hydrodynamic pressures were then calculated at points on the surface of this cylinder with the help of the following formula:

$$\frac{p}{\rho} = -\frac{\partial \phi}{\partial t} - \frac{1}{2}(v_t)^2, \tag{19}$$

where $\phi = \phi^w + \phi^a$ is the sum of the potential ϕ^w for the approaching wave and ϕ^a is an additional potential which is due to the disturbances caused by the cylinder, v_t is the sum of $v_t^w + v_t^a$ and ρ is the density of the water.

The pressure with respect to the squared term has frequencies up to (4ω). It should be noted that if a higher order of Stokes' approximation is used, it changes the values of the components. Because calculations performed with data obtained in experiments show that the terms with frequencies higher than (2ω) are small, the discussion on the experiments is limited up to the double frequency terms.

The pressures at points around the cylinder were integrated numerically to obtain the values of the horizontal and vertical force components.

It is standard practice to consider only the velocities and accelerations at the centre of the cylinder. In the case considered, the radius of the cylinder is small compared with the wave length, and the distance from the cylinder to the bottom is also small compared with the radius of the cylinder. Calculations with normal velocities of the approaching waves which are approximated by the linear term in kR, where k is the wave number, in the power series expansion showed that such approximation is good for values down to $e/R = 1/20$.

In the calculations, it was assumed that the changes in the velocity field caused by the cylinder had a local effect only, without any coupling between the free boundary and the approaching waves. Calculations show that the influence of the bottom is small when the gap is equal to the radius of the cylinder. The biggest gap in the experiment was not greater than 0.40 m. As the water depth was $h = 4.5$ m, the distance to the still water level became more than 3.3 m which was very large compared to the radius of the cylinder $R = 0.40$ m.

The Fourier coefficients and the values of the tangential velocities and pressures on the surface of the cylinder were calculated with the appropriate software prepared in the project.

In Fig. 3, the tangential velocity components are plotted as a space- and time-dependent function for waves with a height of $H = 1.0$ m and a wave period of $T = 4$ s. The water depth was 4.5 m, the cylinder diameter $D = 0.80$ m and the gap width $e = 0.03$ m. The time step was chosen as $T/8$. It must be taken into account that a decreasing gap width causes an increasing velocity; a significant contribution to the pressure through the v_t^2 term should therefore be expected.

The corresponding pressures are plotted in Fig. 4. It is obvious that the v_t^2 term is very important and that a component with the double frequency of the
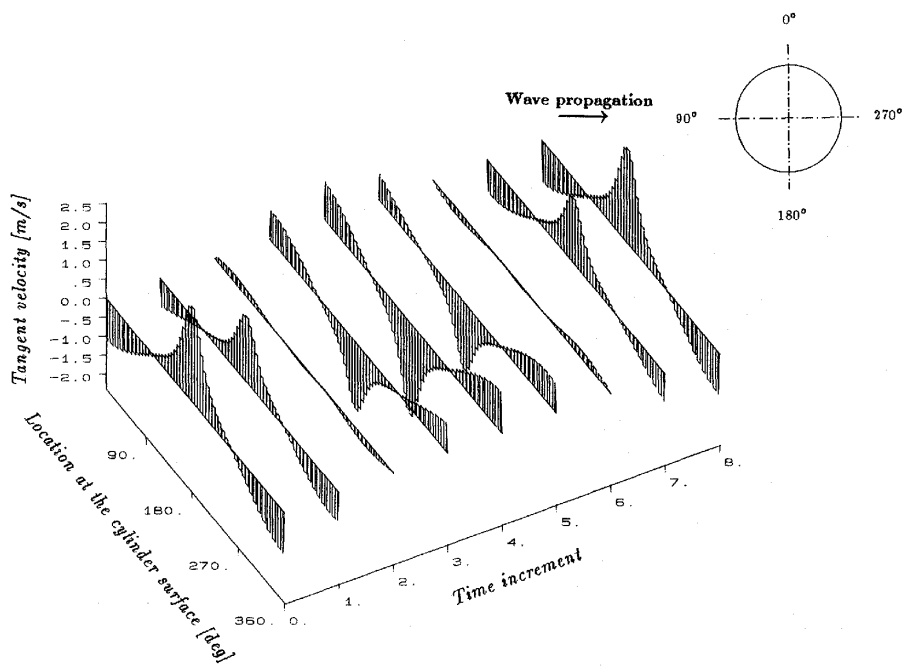
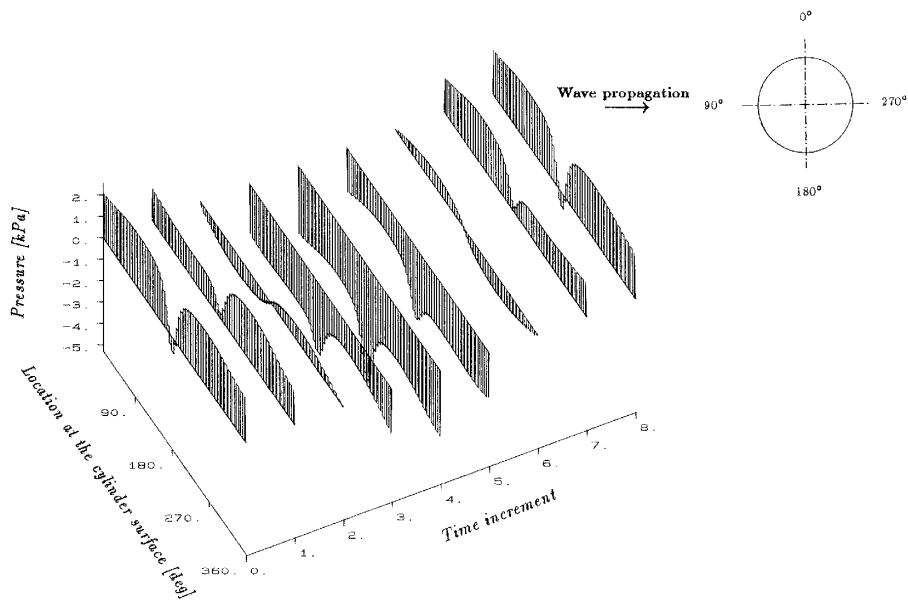**Fig. 3.** Tangent velocities on the surface of the cylinder

Fig. 4. Pressure distribution on the surface of the cylinder

wave appears in the pressure values. It should be noted that the component with double frequency is due to the second term in the Stokes' approximation and due to the square term. The calculations showed that the second influence is dominant with respect to the parameters used in experiments.

In Figs. 5 to 7, the comparison of the theoretical solution with the results of the experiments is given for three gap widths: $e = 0.08$ m, 0.05 m, and 0.02 m. It may be seen that the surface elevation is well described by the second order Stokes' approximation. The drag term of the Morison formula is not included in the theoretical solution of the first component of the horizontal force. The experimental results show a small phase shift and differences in amplitudes which become significant for the very small gap $e/D = 0.025$. There is good conformity for the first component of the vertical force, but the phase shift increases with decreasing gap width for the second component. It can be seen that the potential theory solution gives a reasonable estimation of the amplitudes, whereas the phase shifts cannot be described well. For the small gap $e = 0.02$, the phase shift is considerable and thus the total theoretical diagram of the vertical force does not fit the experimental data. The authors believe that the discrepancy is caused by the dissipation of energy which cannot be considered in the potential theory.
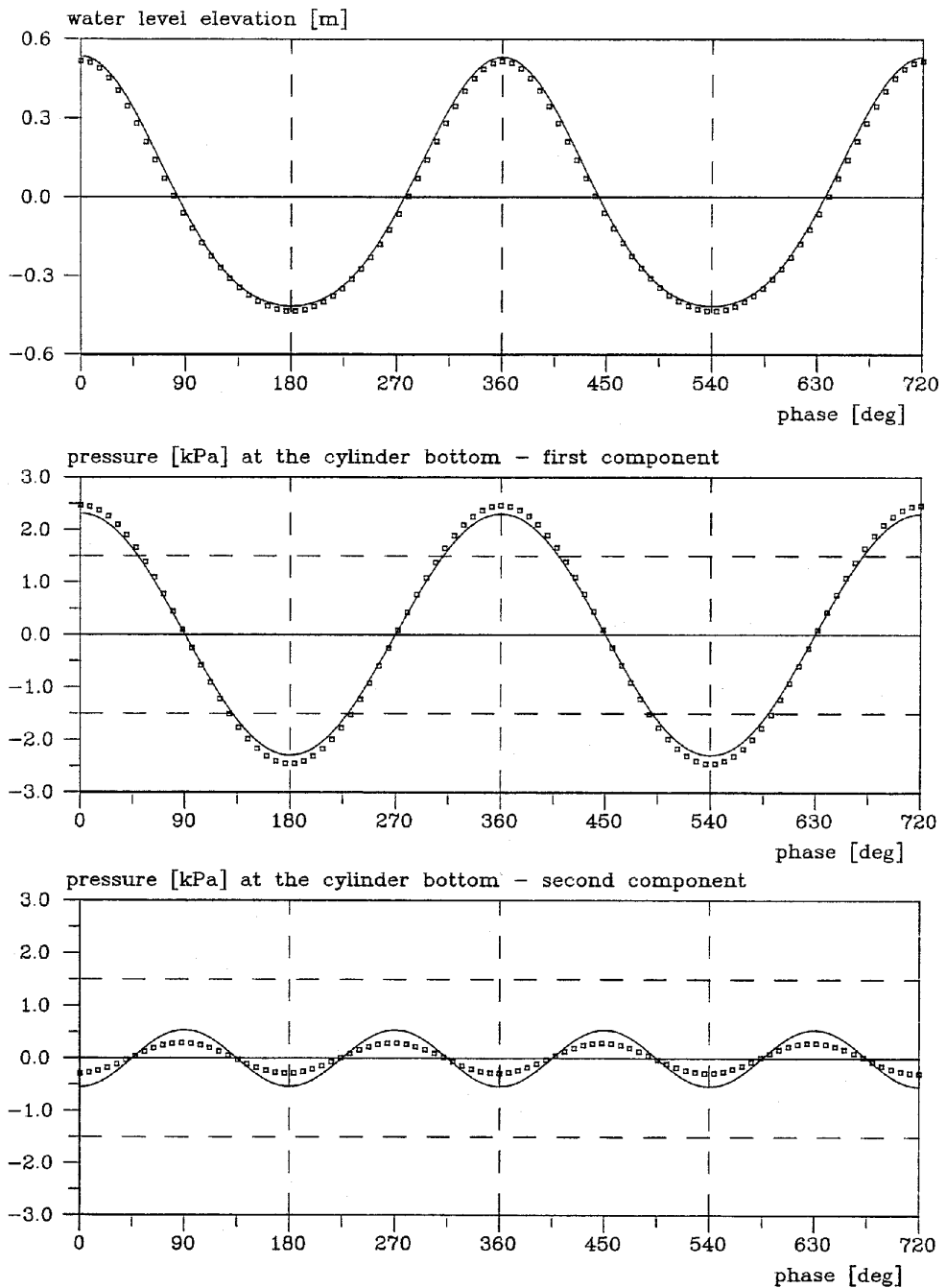
A comparison of theoretical pressures at the bottom of the cylinder shows that the agreement between theoretical and experimental values is good for the first component, but the differences in amplitudes and phase shifts increase when the gap width decreases. The great differences in amplitudes do not correspond to the differences of the resultant vertical forces. It should be remembered that the pressure distribution around the considered point (Fig. 4) is complicated, and a local difference may have little influence on the resultant force. The authors believe that the viscosity for small gaps must have a substantial influence and that it reduces the tangential velocity compared with the calculated values for a perfect fluid with ideal boundary conditions.

4. No Gap Case

When the gap width decreases, the number of significant terms in the Fourier series increases and for very small gaps the obtained numerical results become dubious.
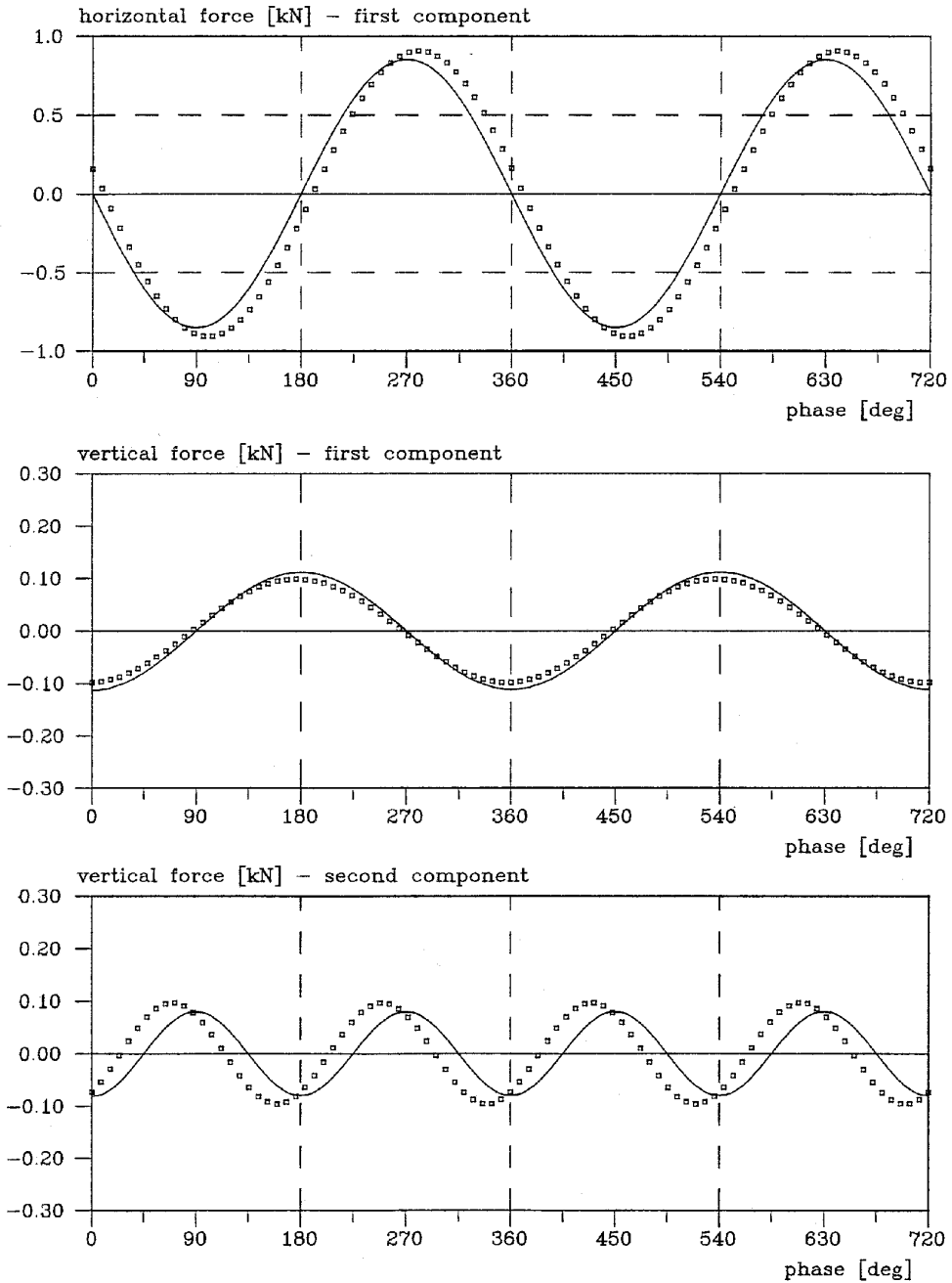
For the limiting case, with $e = 0$, a singularity is existent in the solution at the bottom. For a finite gap, the theoretical solutions are unique and well defined for functions v_n^w due to the velocity field of the Stokes' theory. There is no uniqueness for $e = 0$ if nothing is stated about the type of singularity. The singularity may be defined directly beforehand, but the existence of a solution must be outlined. In a second approach, the singularity is defined by the method of solution. The latter method is used in the present approach and the physical meaning of this singularity is explained.

water level elevation [m]

pressure [kPa] at the cylinder bottom − first component

pressure [kPa] at the cylinder bottom − second component

Wave data: H = 0.95[m]; T = 4.00[s]; d = 4.5[m]; e = 0.08[m]; D = 0.8[m].

Fig. 5a. Comparison of measured data with theoretical solution

horizontal force [kN] — first component

vertical force [kN] — first component

vertical force [kN] — second component

Wave data: H = 0.95[m]; T = 4.00[s]; d = 4.5[m]; e = 0.08[m]; D = 0.8[m].

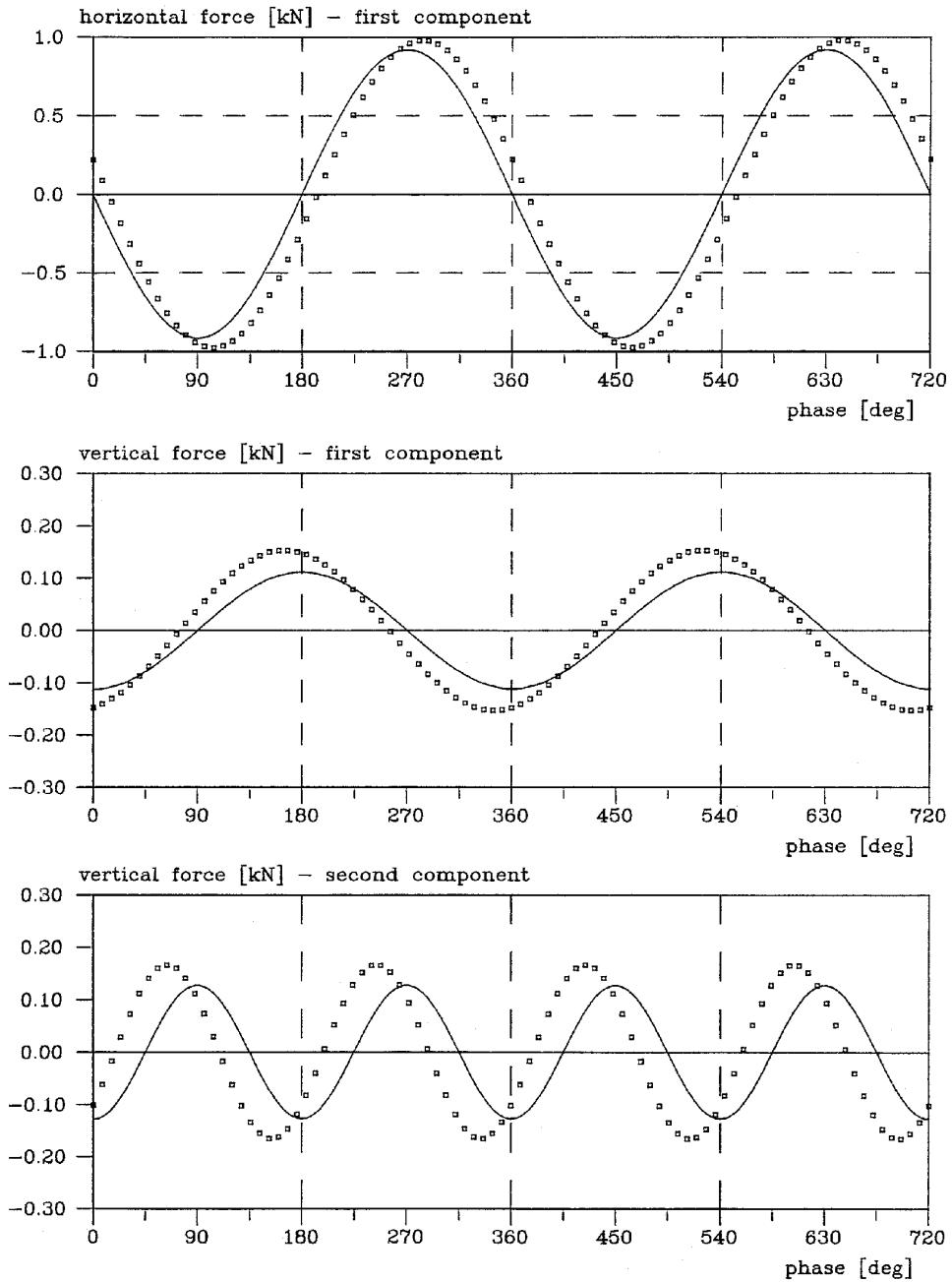**Fig. 5b.** Comparison of measured data with theoretical solution
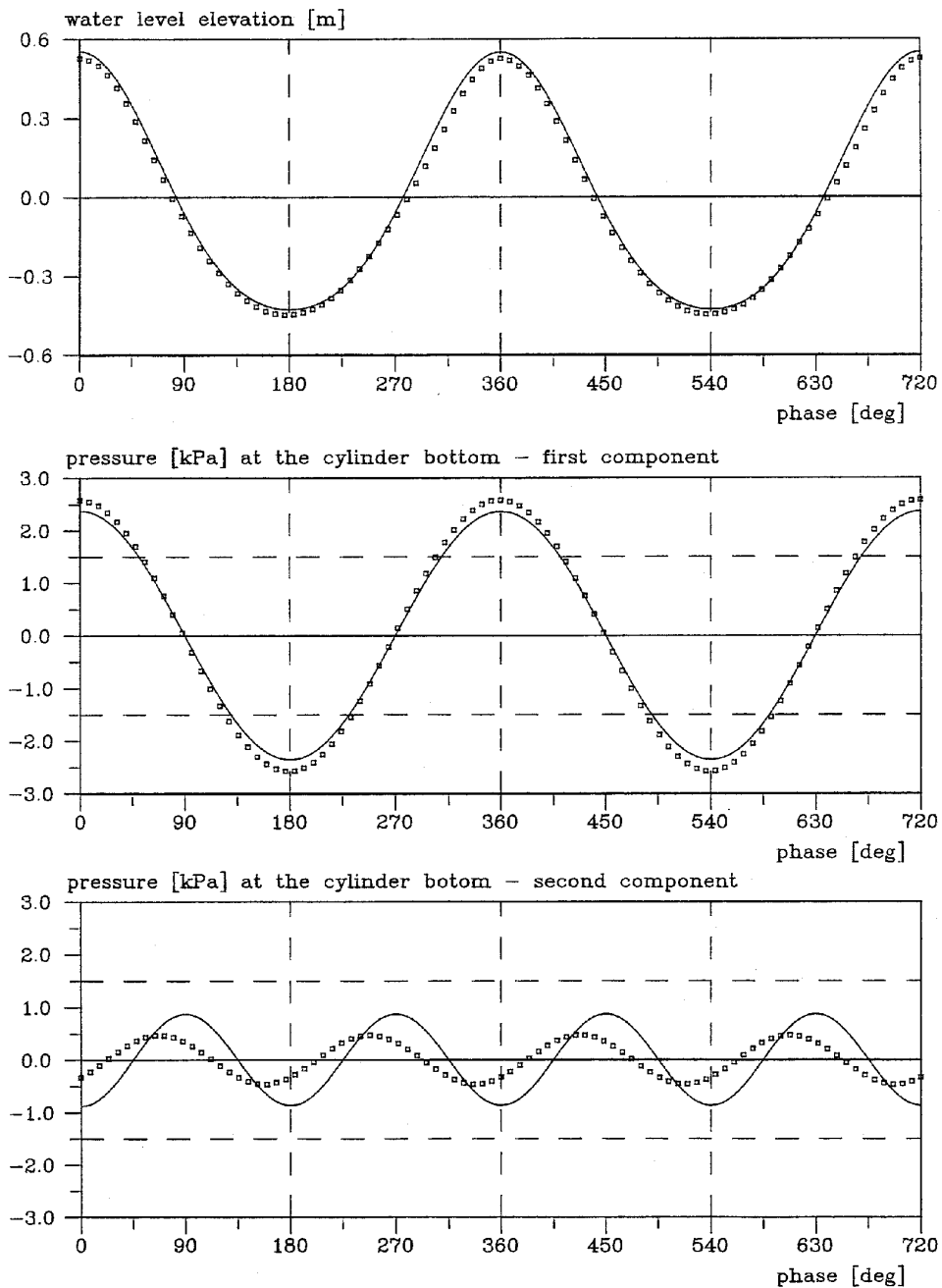
Wave data: H = 0.95[m]; T = 4.00[s]; d = 4.5[m]; e = 0.05[m]; D = 0.8[m].

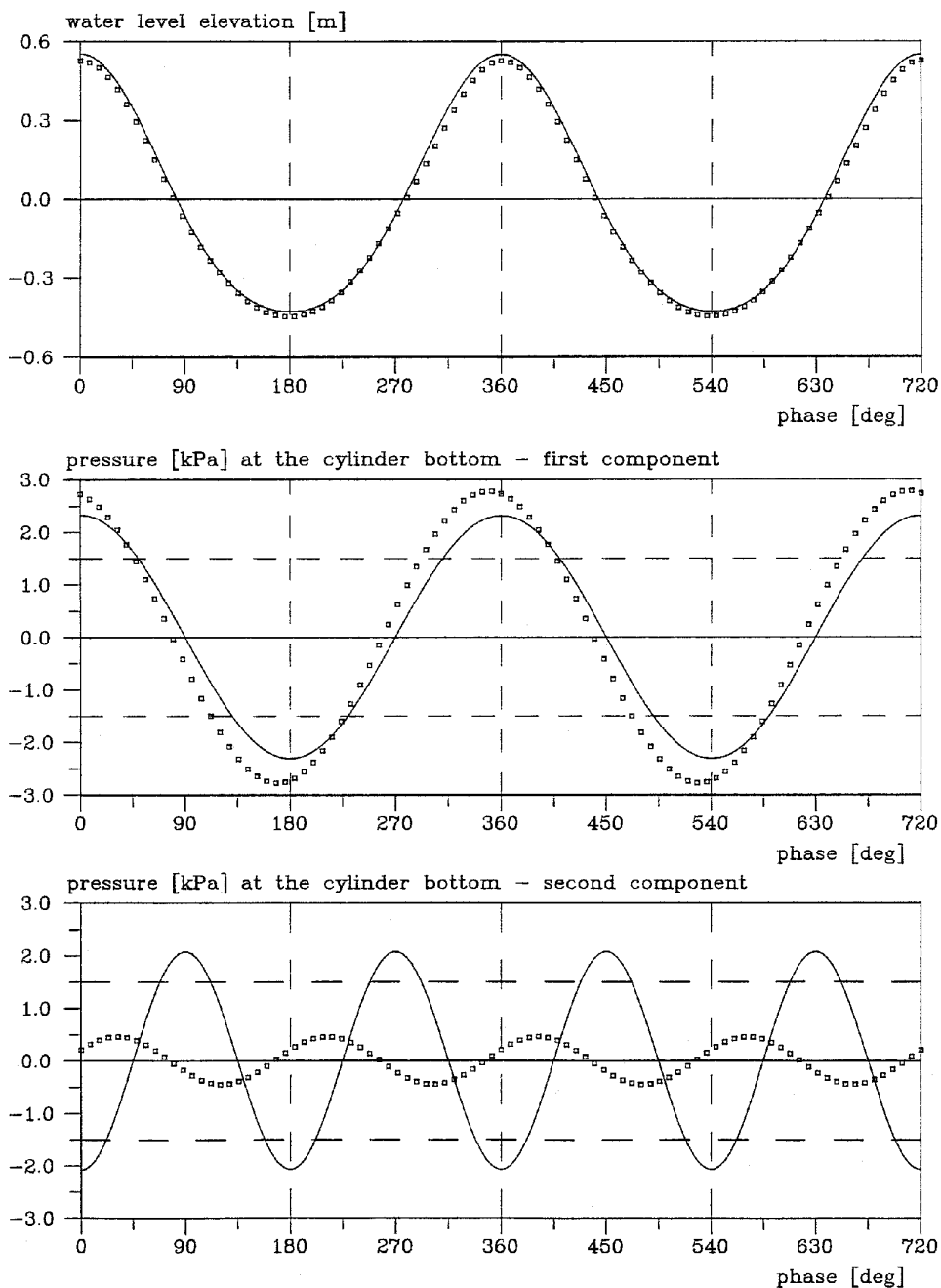**Fig. 6a.** Comparison of measured data with theoretical solution

horizontal force [kN] — first component

vertical force [kN] — first component

vertical force [kN] — second component

Wave data: H = 0.98[m]; T = 4.00[s]; d = 4.5[m]; e = 0.05[m]; D = 0.8[m].

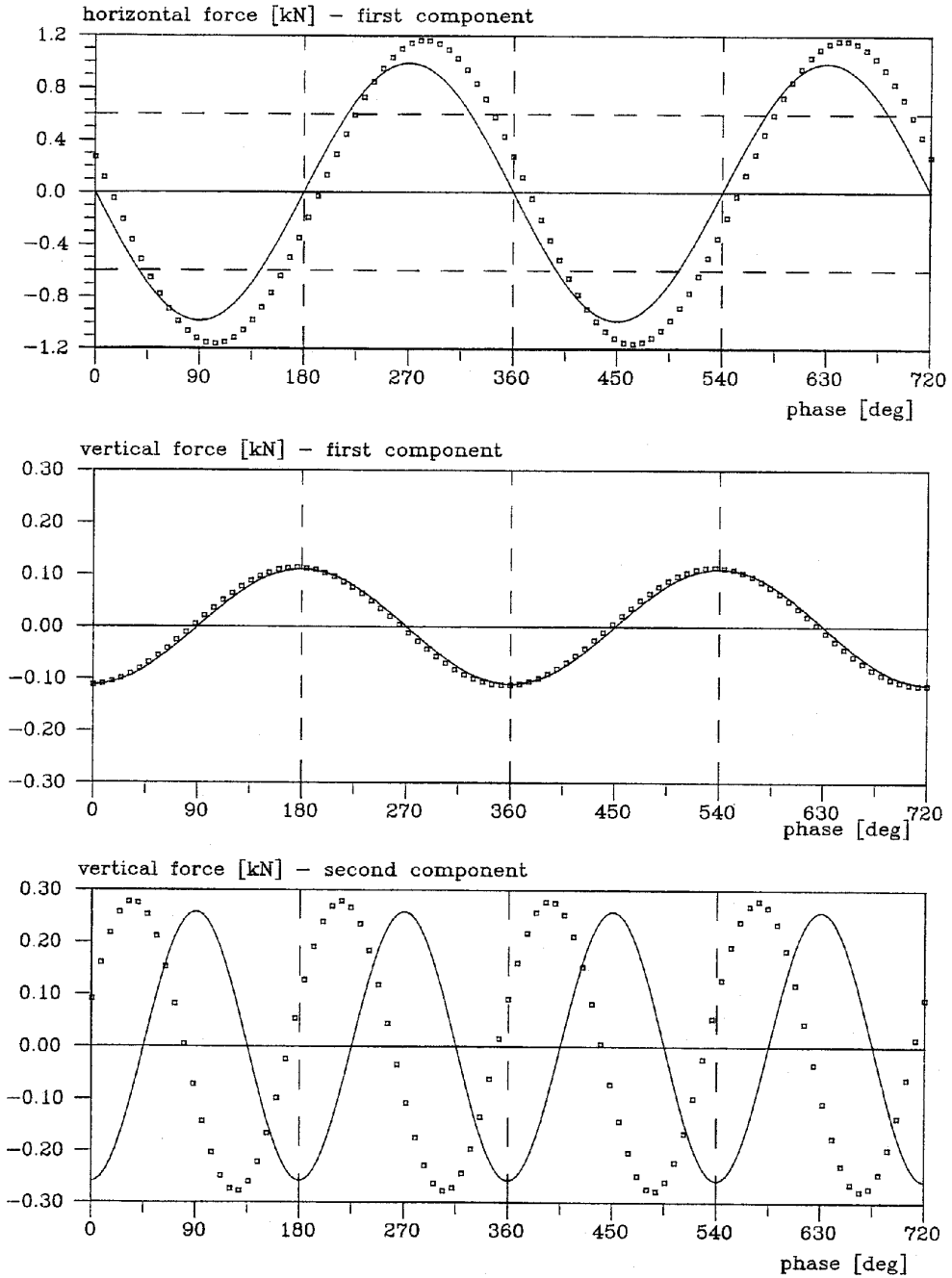**Fig. 6b.** Comparison of measured data with theoretical solution

Wave data: H = 0.98[m]; T = 4.00[s]; d = 4.5[m]; e = 0.02[m]; D = 0.8[m].

Fig. 7a. Comparison of measured data with theoretical solution

horizontal force [kN] — first component

vertical force [kN] — first component

vertical force [kN] — second component

Wave data: H = 0.98[m]; T = 4.00[s]; d = 4.5[m]; e = 0.02[m]; D = 0.8[m].

Fig. 7b. Comparison of measured data with theoretical solution

The velocity field for the approaching wave was expanded in terms of power series around the origin of the x, y coordinate system and only linear terms were retained. For $a = \pi$ it follows that v_n^w is zero. The solution is calculated with the help of the Fourier integrals, and the Fourier transforms are evaluated according to the equation (17), expressing the functions $\sin\alpha$, $\cos\alpha$, $\sin(2\alpha)$, $\cos(2\alpha)$ for v_n^w in terms of v^* by means of the relations (6). The integrals are calculated with the help of the residue theorem, and the inverse transformation is given by the equation (18). In most cases it is not easy, and sometimes not possible, to find a closed form of the solution for the inverse transformation. Then a term appears under the integral, which is equal to $\coth\xi$; this term approaches one for large values of ξ. For that reason, the integral was calculated from zero to M by means of a numerical method and analytically from M to ∞ fixed by the condition that $\coth\xi$ can be replaced by one (M is sufficiently small, i.e. $\cosh M = 1$). The measure of error, as defined before, was of the order of 10^{-4} when the interval from 0 to M had been divided into 1000 parts and M had been chosen sufficiently large.

The values cannot be calculated by the outlined way if $\alpha \to \pi$, $v^* \to \infty$; the limit has to be calculated analytically. For large values of v^*, there is the important contribution to the value of the integral at small values of ξ but the power expansion may be used for small values of ξ. After the expansion is substituted, the integrals are calculated and then the limit is taken for $v^* \to \infty$; this results in:

$$\lim_{v^* \to \infty} \phi(v^*) = -R\omega H \left[\frac{\cos(\omega t)}{\sinh(kh)} + \frac{3kH}{8} \frac{\cos(2\omega t)}{\sinh^4(kh)} \right] \frac{\pi}{2}, \qquad (20)$$

where k is the wave number.

If the same procedure for the case of $v^* \to -\infty$ is applied then the same expression, but with a reversed sign, is obtained. Thus, the singularity at $\alpha = \pi$ corresponds to a finite jump which will appear in the corresponding expressions for the pressures.

If the same procedure is repeated for the tangential velocity components, then the result shows that the additional tangential velocity at $\alpha = \pi$ cancels the corresponding velocities for the approaching wave, and the total velocity becomes zero.

The calculated limits around the point $\alpha = \pi$ characterize the singularity. Physically it can be assumed that the cylinder is welded to the bottom with the consequence that there cannot be any flow from one side to the other; however, there are different pressures on both sides of this imaginary connection. This boundary condition might not be easily achieved in experiments because the pressure differences on both sides tend to a break of water through the contact region.

The solution via Fourier series for finite gaps does not tend to this solution when the gap goes to zero for ideal boundaries.

In order to reveal this problem, it is assumed that a vertical rigid partition wall is installed between the bottom of the cylinder and the bottom of the flume (Fig. 8). The normal velocities are zero, but forces due to pressure differences on both sides of the wall act on the wall. Such a solution should tend to the solution obtained for a cylinder welded to the bottom when $e \rightarrow 0$.
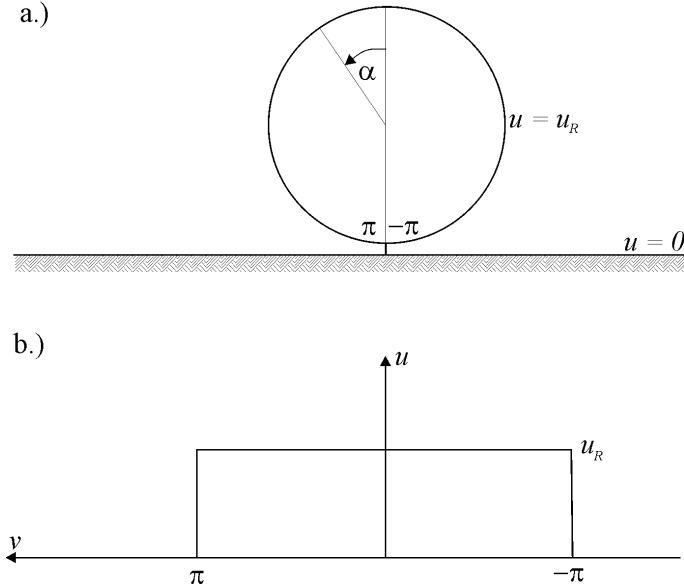

Fig. 8. The cylinder with partition wall

The first step for a solution with respect to this partition wall is to work with a finite gap: the distribution of the tangential velocity components v_t is calculated for $\alpha = \pi$ along the vertical line corresponding to the position of the partition wall, that is from $u = 0$ to $u = u_R$. As a second step, a theoretical solution is constructed with a potential $\phi^*(u, v)$ for which the normal velocities at the cylinder surface and at the bottom are equal to zero and which includes velocities for $v = \pi$ at the partition wall; the velocities calculated in the first step will be eliminated. A suitable solution of the Laplace equation has the following form:

$$\phi^* = A^*v + \sum_{r=1}^{\infty} A_r^* \sinh\left(\frac{r\pi}{u_R}v\right) \cos\left(\frac{r\pi}{u_R}v\right). \tag{21}$$

The coefficients A^*, A_r^* for $r = 1, 2\ldots$ are calculated with the help of numerical integration as presented in the introduction.

In Fig. 9 the amplitudes of components of vertical forces are plotted versus the relative gap e/D (D – diameter of the cylinder). The solid lines represent the solution with a finite gap width. The points shown by stars correspond to the solution $e/D = 0$. It may be seen that the solutions represented by the solid lines do
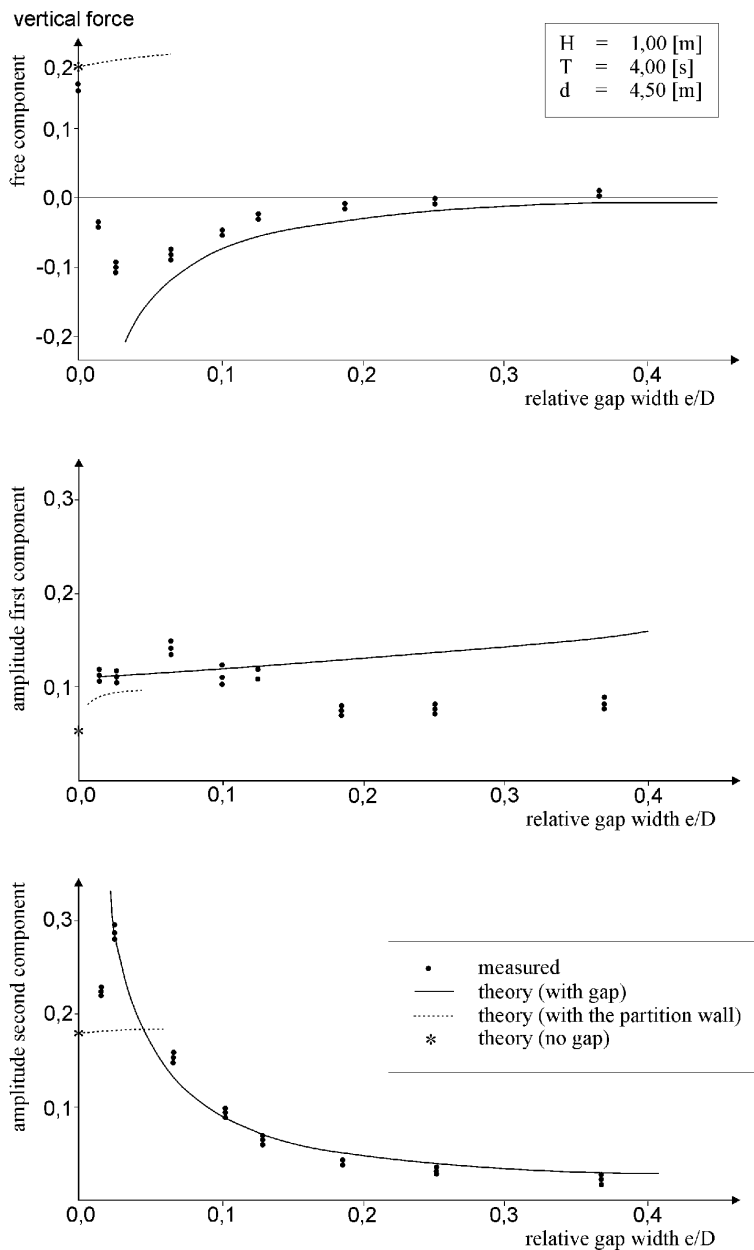
Fig. 9. Amplitudes of component as function of bottom clearance

not approach the points denoted by stars when $e/D \to 0$. The dashed lines represent the relations of a partition wall. The values obtained from experiments are indicated by dots. For the constant included in the time component, the measured values follow the theoretical solution for large values of e/D. The series solution for e/D going to zero diverges. The measured values deviate from the solid line and go to the zero-gap solution.

The amplitude of the first component can be described in a reasonable way by the theoretical solution only for small values of e/D. The differences for $e/D \geq 0.2$ are considerable, and the authors believe that they stem from the assumption of perfect fluid and ideal boundary conditions. The amplitudes of the second component follow the theoretical solution more or less exactly, substantial differences appear only for $e = 0$ and for very small relative gap widths. The calculations show that the constant of the time term and the second component are due to the squared velocity term in pressure. For $e/D > 0.05$, the velocity field obtained from the potential theory offers a good basis for calculating the vertical force component.

The introduction of a partition wall does not describe the dynamical behaviour of a cylinder for small gaps when the viscosity of the fluid is of primary importance. It can be noted from the results of this elaboration that the pressure distribution in the neighbourhood of small gaps is sensitive to local boundary conditions.

It is interesting to note that for $e/D > 0.02$ the constant included in the time component of the vertical force acts downwards, while for $e/D = 0$ it acts upwards.

The solution of the case with partition wall has no direct technical meaning, but it shows how sensitive the solutions are. For small gaps, viscosity should diminish the velocity in the fluid and behaviour similar to that introduced by the installation of the partition wall could be expected. If the pipe is laid on a seabed, the natural conditions of the contact are of a random nature and thus one may expect complicated three dimensional behaviour.

When one thinks about design formulae as proposed by Bowie (1977), in an interesting range of e/D – results of the presented analysis show that the constant included in the time term and the amplitude of the component with the double frequency of the wave, may be calculated from potential theory with reasonable accuracy.

5. Conclusions

The theoretical solution based on the potential theory of incompressible perfect fluids and ideal boundary conditions gives a useful description of the wave-induced pressures on the surface of a cylinder as far as the amplitudes of the time-dependent components are concerned. The increase of the pressure near the gap is described well, when compared with experimental results.

The pressure distribution near small gaps is very sensitive to local boundary conditions. The solution for a finite gap does not go uniformly to the limiting case when there is no gap at the bottom.

The phase shifts with respect to the waves are poorly described by the potential theory. The suggestion is that the dissipation of energy due to viscosity and vortex shedding, which cannot be described by the applied potential theory, plays an important role.

The resultant horizontal force component is not as sensitive to the local conditions near the gap as the vertical force component, and a solution for finite gaps goes uniformly over to the limiting case of no gap. The potential theory gives a good estimate of the influence of the e/D parameter on the inertia term in the Morison formula.

The squared velocity term in the pressures is important for the resultant vertical forces. The potential theory solution gives a good estimate of the amplitude components due to this term. The phase shift must be taken from experiments, and it is plausible that it may be estimated when viscous effects are considered.

References

Bowie L. G. (1977), *Forces Exerted by Waves on a Pipeline at or Near the Ocean Bottom*, Technical paper No. 77–11, US Army, Corps of Engineers, Coastal Engineering Research Centr.

Carpenter L. H. (1958), On the motion of two cylinders in an ideal fluid, *Journal of Research of the National Bureau of Standards,* Vol. 61, No. 2, 83–87.

Chakrabarti S. K. (1987), *Hydrodynamics of Offshore Structures*, Computational Mechanics Publications, Springer Verlag, Berlin, Heidelberg.

Moon P., Spencer D. E. (1971), *Field Theory Handbook*, Springer Verlag, Berlin, Heidelberg, New York.

Müller W. (1928), *Matematische Strömungslehre*, Springer Verlag, Berlin.

Sarpkaya T., Isaacson M. (1981), *Mechanics of Wave Forces on Offshore Structures*, Van Nostrand Reinhold Company, New York.

Sumer B. M., Fredsøe J. (1997), *Hydrodynamics around Cylindrical Structures*, Advanced Series on Ocean Engineering, Vol. 12, World Scientific.

Wright J. C. Yamamoto T. (1979), Wave forces on cylinders near plane boundaries, *Journal of Waterways, Port, Coastal and Ocean Division ASCE*, Vol. 101, No. WW 1, 1–13.

Yamamoto T., Nath J. H., Slotta L. S. (1974), Wave forces on cylinders near plane boundary, *Journal of Waterways, Port, Coastal and Ocean Division ASCE*, Vol. 100, No. 4, 345–359.